JCTC Journal of Chemical Theory and Computation

Excited State Potential Energy Surfaces of Polyenes and Protonated Schiff Bases

Robert Send*

Institut für Physikalische Chemie, Universität Karlsruhe, Kaiserstrasse 12, D-76128 Karlsruhe, Germany

Dage Sundholm

Department of Chemistry, P.O. Box 55 (A.I. Virtanens plats 1), University of Helsinki, FI-00014 Helsinki, Finland

Mikael P. Johansson

Lundbeck Foundation Centre for Theoretical Chemistry, Aarhus University, Langelandsgade 140, DK-8000 Århus C, Denmark

Filip Pawłowski

Physics Institute, Kazimierz Wielki University, Plac Weyssenhoffa 11, PL-85-072 Bydgoszcz, Poland

Received May 14, 2009

Abstract: The potential energy surface of the ^1B_u and $^1A'$ states of all-*trans*-polyenes and the corresponding protonated Schiff bases have been studied at density functional theory and coupled cluster levels. Linear polyenes and protonated Schiff bases with 4 to 12 heavy atoms have been investigated. The calculations show remarkable differences in the excited state potential energy surfaces of the polyenes and the protonated Schiff bases. The excited states of the polyenes exhibit high torsion barriers for single-bond twists and low torsion barriers for double-bond twists. The protonated Schiff bases, on the other hand, are very flexible molecules in the first excited state with low or vanishing torsion barriers for both single and double bonds. Calculations at density functional theory and coupled cluster levels yield qualitatively similar potential energy surfaces. However, significant differences are found for some single-bond torsions in longer protonated Schiff bases, which indicate a flaw of the employed time-dependent density functional theory methods. The close agreement between the approximate second and third order coupled cluster levels indicates that for these systems calculations at second order coupled cluster level are useful in the validation of results based on time-dependent density functional theory.

1. Introduction

The 11-*cis*-retinal photoreceptor in rhodopsin is responsible for the 11-*cis* to all-*trans* isomerization reaction which triggers the human visual process. The absorption of a photon initiates a complex and fast photoreaction involving several intermediates; the first species are formed within 200 fs.[1−9] The product of the photoisomerization reaction after about 1 ps is bathorhodopsin which has a distorted all-*trans* structure.[8−10] Experimental information about the photoreaction mechanism can be obtained by, e.g., femtosecond Raman spectroscopy (FSRS) measurements,[9] but computational approaches are indispensable to complement the experimental results.

The size of the full retinal still poses something of a challenge for accurate computational approaches. Insight

* Corresponding author e-mail: robert.send@kit.edu.

10.1021/ct900240s CCC: $40.75
Published on Web 07/27/2009

gained from the study of smaller model systems, the focus of the present study, alleviates to some extent this problem. All-*trans* polyenes and the corresponding protonated Schiff bases (PSBs), where one $=CH_2$ end group is replaced by the isoelectronic $=NH_2^+$, are often adopted as models for retinal PSB chromophores[11−16] It has to be kept in mind that the polyenes and the PSBs have different properties,[13] and molecular orbital theory models based on polyenes cannot be used to understand the excited state behavior of the PSBs.

Computationally demanding approaches such as complete-active-space self-consistent-field (CASSCF)[17] calculations in combination with second order perturbation theory (CASPT2) corrections[18] have been considered the most reliable approach for computational studies of the retinal isomerization reaction. However, the CASSCF/CASPT2 approach suffers from some undesired limitations. At the CASSCF level, merely the static valence correlation effects are considered, because only a few valence orbitals and electrons can be included in the active space. Dynamic electron correlation effects can be taken into account in a subsequent CASPT2 calculation. Larger active spaces could be used in multireference calculations by employing the restricted active space SCF method (RASSCF)[19] which also can be augmented with the second-order perturbation theory (RASPT2) approach[20] for considering parts of the remaining dynamical correlation effects. Due to the high computational cost, the molecular structure is usually not optimized at the CASPT2 level. Using CASSCF structures can lead to very large errors in the computed excitation energies, as recently confirmed by Altun et al.[21] Further, the employed basis sets are generally only of double-ζ quality, which is somewhat inadequate for reliable energetics at correlated *ab initio* levels.[22−26] Basis set studies on acrolein, *cis*-butadiene, and diazomethane show that also the CASPT2 geometries are strongly basis set dependent, with large differences between double and triple-ζ results.[27]

Alternative computational approaches for retinal studies are necessary to allow excited state optimizations using analytical gradients and larger basis sets. The time-dependent density functional theory (TDDFT) approach[28−32] has proven to be a successful method for studies of excited states. Optimizations can be routinely performed as effective algorithms for molecular gradients have been developed and implemented.[33] We also note that recent developments within the "dressed TDDFT" approach[34−37] appear to be promising for treating double-excitation dominated transitions, which are troublesome for standard TDDFT approaches. However, extensive TDDFT calculations on retinal protonated Schiff-bases (PSBs) using large basis sets have yielded results in disagreement with previously published CASSCF/CASPT2 studies.[22,23,38−41] The molecular structure of the first excited state of retinal PSBs optimized at the TDDFT level has a long single bond connecting the β-ionone ring with the retinyl chain, leading to a $-90°$ orientation of the ring relative to the retinyl chain. For the ground state structure there is only a $-39°$ twist angle between the ring and the chain.[38] Such a structure of the first excited state is not supported at any other level of theory. The most popular explanation for these discrepancies is the inability of the TDDFT method to accurately describe long-range charge transfer effects,[42,43] a conception that is challenged by this work.

Coupled cluster methods offer an alternative to the above-mentioned computational procedures. The approximate second order coupled cluster approach (CC2) is still feasible for molecules as large as retinal and accounts for a significant amount of electron correlation effects.[44,45] It has an appealing black-box character and allows excited state optimizations with large basis sets using analytical gradients. The CC2 method is able to accurately describe excited states with dominant single excitation character. CC2 calculations on retinal PSBs indicated that this necessary condition holds for at least the two lowest excited states;[39] the CC2 excitation energies deviate less than 0.07 eV from available experimental data.[46] The CC2 method does not suffer from long-range charge transfer problems since the exact-exchange operator is employed. The accuracy of CC2 calculations can be further assessed at the computationally more demanding approximate third order coupled cluster (CC3) level[47] on smaller PSB model compounds.

Recent CC2 and TDDFT studies on the 11-*cis* retinal PSB yielded qualitatively the same results for excitation energies, excited state molecular structures, dipole moment changes on excitation, and for twists along two major reaction coordinates.[38−40,48] The CC2 and TDDFT studies proposed a new isomerization reaction mechanism supported by femtosecond spectroscopic studies.[9] The reaction involves twisted retinyl structures and a stable intermediate.[41] The main disagreement between the results obtained at the two levels concerns the torsion angle of the single bond connecting the retinyl chain with the β-ionone ring moiety. Zaari and Wong also noted discrepancies between the TDDFT and CC2 description of some excited states of retinal.[49] The objective of the present study is to perform a thorough benchmark comparison of the TDDFT and CC2 results.

Although not central to this study, and therefore addressed only briefly, another discrepancy between the CC2 and TDDFT results on the one side, and the CAS results on the other side, is found in the excited state bond length alternation. CASSCF calculations on PSBs by Page and Olivucci yielded excited state structures with an inverted bond length alternation as compared to the ground state;[27] the double bonds become longer and the single bonds shorter upon excitation. The inverted bond length alternation is less severe at the CASPT2 level. It was also found that the potential energy surface (PES) of the excited state of PSBs is flat. At the CASSCF level, the authors obtained two energetically almost degenerate geometries for the 2,4-pentadieniminium cation with an essentially reversed bond conjugation, whereas at the CASPT2 level only one minimum is obtained.[27] In contrast, at the CC2 and TDDFT levels, the bond length alternation in the excited state of the 11-*cis* retinal PSB is not inverted but enhanced; the double bonds become shorter and the single bonds longer.[14,40] Before studying the bond length discrepancy in detail, it is necessary to analyze the differences between the CC2 and TDDFT results, and we therefore

concentrate on the PESs of bond torsion twists at the CC2 and TDDFT level.

Here, we present systematic TDDFT and CC2 studies of the PESs of the first excited state for both single and double bonds of the polyenes and the PSBs. The CC3 method is used to assess the accuracy and the reliability of the CC2 calculations. If the MR character is important, the PESs obtained at the CC2 and CC3 levels significantly differ. This occurs especially for large torsion angles of the double bond twists. The energies in these regions are not well-described by the single-reference methods employed in this study but are at the same time of little importance for the discussion and conclusions, which only consider small-angle twists. Previous work has shown that as long as the structural region of interest is located far from a conical intersection, the performance of, e.g., CC2 is very satisfactory.[50,51]

The PESs are examined by performing single point calculations for torsion angles of the carbon−carbon (carbon−nitrogen) bonds yielding upper bounds for the torsion barriers. Relaxation of the remaining structural degrees of freedom would introduce unpredictable uncertainties. For some molecules, a remote part of the molecule might twist, whereas in other cases a small barrier can prevent such relaxations. Thus, significantly different results can be obtained for two molecules even though the differences in the PESs are small.

The present article is structured as follows. After an overview of the computational methods employed, Section 3 discusses basis set effects on the vertical excitation energies and the PESs as well as basis set effects on the bond length alternation of the ground and the first excited state. In Section 4, the performance of different density functionals is reported. The PESs of the polyenes and the PSBs calculated at the TDDFT, CC2, and CC3 levels are compared in Section 5.

2. Computational Details

2.1. Basis Sets. The basis set convergence of the excitation energies is investigated at the CC2 level by performing single point calculations using a systematic sequence of Dunning's correlation-consistent (cc) basis sets up to aug-cc-pV6Z quality.[52−54] In the corresponding B3LYP[55,56] TDDFT calculations, Dunning's cc basis sets up to aug-cc-pVQZ are employed. We also used the Karlsruhe basis sets of split valence quality with polarization functions on all atoms (SVP) and on all atoms except hydrogens (SV(P)),[57] the triple-ζ valence quality basis set with one (TZVP) and two (TZVPP) sets of polarization functions,[58,59] and the quadruple-ζ basis sets augmented with two sets of polarization functions (QZVPP).[60] The basis sets denoted aug-SV(P) are the SV(P) basis sets augmented with diffuse functions from Dunning's cc double-ζ basis sets (aug-cc-pVDZ). The aug-TZVP basis sets are the TZVP basis sets augmented with the diffuse functions from Dunning's cc triple-ζ basis sets (aug-cc-pVTZ).

2.2. Functionals. The performance of different density functionals is assessed by single point TDDFT calculations using functionals of the generalized gradient approximation (GGA) as well as hybrid functionals. We have used the BP86[61−63] and PBE[64] GGA functionals as well as the B3LYP[55,56] and PBE0[65] hybrid GGA functionals. The Coulomb-attenuated B3LYP (CAM-B3LYP) functional[66] was used to check the long-range charge transfer effects on the excitation energies. In the benchmark calculations of the functionals, the TZVPP basis set was used; in the CAM-B3LYP calculations, the cc-pVTZ basis set was employed.

2.3. Ground State Structures. In the density functional theory (DFT) studies, the ground state structures were optimized using the B3LYP functional and the TZVPP basis sets. For the excited state coupled cluster studies, the ground state structures were optimized at the second order Møller−Plesset (MP2) perturbation theory level using the resolution-of-identity (RI) approximation[67−69] and the TZVPP basis sets. The optimized Cartesian coordinates are given in Sections I and II of the Supporting Information (SI).

2.4. Excited State Potential Energy Surfaces. The B3LYP ground state structures were starting geometries for calculations at the TDDFT level. The MP2 structures were starting geometries for calculations at the CC2 and CC3 levels. At the CC2 level,[44] the RI approximation is employed to speed up the calculations.[45] CC3 is an iterative approximation to the coupled cluster singles, doubles, and triples (CCSDT) model.[47] The triples equation is approximated according to two criteria: (i) the triples equation is restricted to contain only terms that enter to second order in the fluctuation potential; (ii) the single excitations are treated as zeroth order parameters in the fluctuation potential. Keeping all terms that enter to second order in the fluctuation potential leads to an energy that is correct through fourth order.[47] An error analysis of the CC3 excitation energies has shown that the excitation energies of single-replacement dominated states are correct through third order.[44,70,71] This places CC3 between the CCSDT model and the coupled cluster singles and doubles (CCSD) and CC2 models. The excitation energies of double-replacement dominated states are correct in CC3 through second order,[70,71] which is the same as in the case of CCSDT.

The PESs were examined by twisting the ground state structure around all carbon−carbon (carbon−nitrogen) bond torsion coordinates. Energies of the ground and first excited state are obtained in single point calculations at intervals of 15° for each torsion angle.

2.5. Programs and Nomenclature. The CC3 and CAM-B3LYP calculations were carried out using a development version of the Dalton program package.[72] All other calculations were done with the Turbomole package, versions V5−9 and V5−10.[73] Difference density plots were produced with the gOpenMol package.[74,75]

In the following, we denote the polyenes by POLx and the protonated Schiff bases by PSBx, where x is the number of heavy atoms. The systematic chemical names and a figure with the corresponding structures are given in Section III of the SI. All PESs discussed in this work refer to the first excited states of either ^1B_u or $^1A'$ symmetry. We denote bond torsion curves repulsive, when the energy of the planar structure is lower than

Table 1. Basis Set Convergence of the 1^1B_u and 2^1A_g Excitation Energies (EE in eV) for POL4 (*trans*-1,3-Butadiene) Calculated at the CC2 Level using Dunning's Correlation-Consistent Basis Sets and the Karlsruhe Basis Sets[b]

basis set	EE(1^1B_u)	ΔEE(1^1B_u)	EE($2\,^1A_g$)	ΔEE($2\,^1A_g$)
cc-pVDZ	6.664		7.952	
cc-pVTZ	6.439		7.685	
cc-pVQZ	6.349		7.536	
cc-pV5Z	6.265		7.372	
cc-pV6Z	6.222		7.272	
aug-cc-pVDZ	6.165	−0.499	7.062	−0.890
aug-cc-pVTZ	6.156	−0.283	7.077	−0.608
aug-cc-pVQZ[a]	6.158	−0.191	7.081	−0.455
aug-cc-pV5Z	6.158	−0.108	7.074	−0.297
aug-cc-pV6Z	6.156	−0.065	7.071	−0.201
SV(P)	6.780		8.041	
SVP	6.743		7.996	
TZVP	6.508		7.662	
TZVPP	6.369		7.570	
QZVPP	6.273		7.389	
aug-TZVP	6.171	−0.337	7.054	
aug-TZVPP	6.157	−0.212	7.081	

[a] The excitation energies obtained with all electrons correlated are 6.162 and 7.091 eV, for $1\,^1B_u$ and $2\,^1A_g$, respectively. [b] The $1s_C$ orbitals are uncorrelated. The contributions from the diffuse basis functions (ΔEE in eV) are also given.

the energy of the perpendicular structure, and attractive, when the energy of the planar structure is higher than the energy of the perpendicular structure. The curvature of the PES at the planar orientation can either be convex yielding higher energies for slightly twisted structures or concave yielding lower energies for slightly twisted structures.

3. Basis Set Effects

3.1. Excitation Energies. The basis set requirements are tested by performing CC2 and B3LYP TDDFT calculations on the 1^1B_u and 2^1A_g states of POL4 and on the $2^1A'$ and $1^1A''$ states of PSB4. The CC2 excitation energies are given in Tables 1 and 2, and the B3LYP excitation energies are given in Tables 3 and 4.

For POL4, diffuse basis functions are necessary to reach the basis set limit at the CC2 and B3LYP level; they also speed up the basis set convergence. The CC2/aug-cc-pVTZ excitation energies deviate only a few meV from the CC2 limit obtained in the CC2/aug-cc-pV6Z calculation. The contributions from diffuse functions to the CC2/aug-cc-pV6Z excitation energies are 0.06 and 0.2 eV.

For PSB4, diffuse basis functions are less important. This is expected as the molecular orbitals in the cationic PSBs are more strongly bound than in the neutral polyenes. The use of diffuse functions gives almost the same excitation energies as basis sets of the next Cardinal number. The cc-pVTZ excitation energies agree within 0.1 eV with the excitation energies calculated at the CC2/cc-pV6Z levels.

The cc-pVTZ basis set is the most cost efficient cc basis set for the PSBs, whereas already the aug-cc-pVDZ basis set seems to be appropriate for the polyenes. Calculations using the augmented Karlsruhe basis sets yield excitation energies of comparable accuracy as the corresponding Dunning basis sets.

Table 2. Basis Set Convergence of the $2^1A'$ and $1^1A''$ Excitation Energies (EE in eV) for PSB4 (the *trans*-2-Propeniminium Cation) Calculated at the CC2 Level using Dunning's Correlation-Consistent Basis Sets and Karlsruhe Basis Sets[b]

basis set	EE($2^1A'$)	ΔEE($2^1A'$)	EE($1^1A''$)	ΔEE($1^1A''$)
cc-pVDZ	5.916		7.388	
cc-pVTZ	5.780		7.241	
cc-pVQZ	5.736		7.201	
cc-pV5Z	5.712		7.185	
cc-pV6Z	5.705		7.179	
aug-cc-pVDZ	5.760	−0.155	7.278	−0.110
aug-cc-pVTZ	5.714	−0.066	7.194	−0.046
aug-cc-pVQZ[a]	5.706	−0.030	7.182	−0.019
aug-cc-pV5Z	5.703	−0.009	7.178	−0.007
SV(P)	5.950		7.370	
SVP	5.911		7.396	
TZVP	5.787		7.355	
TZVPP	5.756		7.225	
QZVPP	5.718		7.193	
aug-TZVP	5.729	−0.058	7.228	
aug-TZVPP	5.714	−0.042	7.192	

[a] The excitation energies obtained with all electrons correlated are 5.698 and 7.165 eV for $2\,^1A'$ and $1\,^1A''$, respectively. [b] The $1s_C$ and $1s_N$ orbitals are uncorrelated. The contributions from the diffuse basis functions (ΔEE in eV) are also given.

Table 3. Basis Set Convergence of the 1^1B_u and 2^1A_g Excitation Energies (EE in eV) for POL4 (*trans*-1,3-Butadiene) Calculated at the B3LYP TDDFT Level using Dunning's Correlation-Consistent Basis Sets[a]

basis set	EE(1^1B_u)	ΔEE(1^1B_u)	EE(2^1A_g)	ΔEE(2^1A_g)
cc-pVDZ	5.996		7.162	
cc-pVTZ	5.857		7.002	
cc-pVQZ	5.788		6.891	
aug-cc-pVDZ	5.626	−0.370	6.561	−0.601
aug-cc-pVTZ	5.613	−0.244	6.543	−0.459
aug-cc-pVQZ	5.607	−0.181	6.528	−0.363

[a] The contributions from the diffuse basis functions (ΔEE in eV) are also given.

Table 4. Basis Set Convergence of the $2^1A'$ and $1^1A''$ Excitation Energies (EE in eV) for PSB4 (the *trans*-2-Propeniminium Cation) Calculated at the B3LYP TDDFT Level using Dunning's Correlation-Consistent Basis Sets[a]

basis set	EE($2^1A'$)	ΔEE($2^1A'$)	EE($1^1A''$)	ΔEE($1^1A''$)
cc-pVDZ	5.796		6.385	
cc-pVTZ	5.726		6.355	
cc-pVQZ	5.699		6.344	
aug-cc-pVDZ	5.677	−0.119	6.329	−0.056
aug-cc-pVTZ	5.673	−0.053	6.334	−0.021
aug-cc-pVQZ	5.673	−0.027	6.334	−0.010

[a] The contribution from the diffuse basis functions (ΔEE in eV) are also given.

The TDDFT excitation energies converge somewhat faster toward the basis set limit compared to the CC2 ones, though the difference is small. With diffuse basis functions, the CC2 and TDDFT calculations exhibit a similar basis set convergence. Other uncertainties such as the errors of the numerical integration might become significant, as the differences between the excitation energies using basis sets of different Cardinal numbers are very small. A systematic study of the basis set requirements for calculation of the electronic

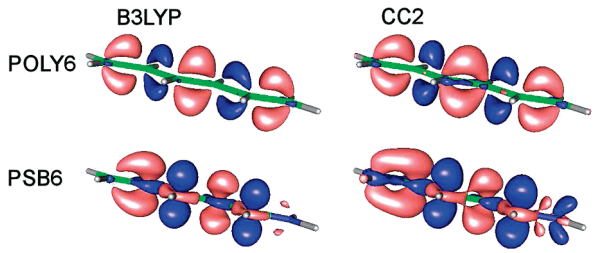

Figure 1. Density differences between the ground states of POL6 and PSB6, compared to the first excited states of ^1B_u and $^1A'$ symmetry, calculated for the planar conformations. The calculations were performed at both B3LYP and CC2 levels, using the aug-cc-pVTZ basis set. Light red color represents regions of electron loss upon excitation; dark blue represents regions of electron gain. An isocontour value of 0.003 e has been used throughout.

excitation spectra of POL4 and PSB4 will be published separately.[76]

Molecular structure effects on the excitation energies can be as large as 0.1 eV. For example, the CC2/aug-cc-pVTZ calculation on PSB6 using a BP86/TZVP structure yields the two lowest excitation energies of 5.613 and 7.052 eV, with the MP2/TZVPP structure one gets excitation energies of 5.714 and 7.194 eV. Using the more accurate MP2/TZVPP structure leads to slightly larger excitation energies than at the BP86/TZVP level. At the BP86 level, the double bonds are about 1 pm longer than the MP2 distances, whereas the single bonds obtained at the two levels are practically equal. Thus, the use of accurate molecular structures is important when aiming at very accurate vertical excitation energies.

3.2. Potential Energy Surfaces. In contrast to the excitation energies, the PESs of the first excited state of POL6 and PSB6 show rather similar basis set dependencies. Cancellation of errors seems to make diffuse basis functions less important for the PESs than for the excitation energies. The basis set convergence is faster at both the CC2 and B3LYP levels. Graphs of the basis set studies at the CC2 and B3LYP levels are given in Section IV of the SI.

Torsion barriers are practically independent of the basis set size at both computational levels. Twisted structures have a somewhat larger basis set dependence than the planar ones. The basis set dependence at the TDDFT level is somewhat smaller than at the CC2 level.

CC3 calculations on POL4 and PSB4 using Dunning's cc-pVDZ, aug-cc-pVDZ, and cc-pVTZ basis sets show a very similar basis set dependence as obtained at the CC2 level. Thus, the PESs calculated at the CC3/cc-pVDZ level can be used for benchmarking results obtained with computational levels that consider electron correlation less accurately. Graphs displaying the basis set dependence of the PESs at the CC3 level can be found in the Section V of the SI.

The methods employed in this study have difficulties in describing molecules with practically perpendicular bond orientations, where the single-configuration dominance breaks down. It should therefore be noted that the energies of the strongly distorted structures are unreliable and included for completeness. Tables with the minimum and maximum $\mathcal{T}_1$ diagnostic values[77] for the bond twists of all polyenes and PSBs can be found in Section VI of the SI.

3.3. Ground and Excited State Optimization. The first excited state of polyenes and PSBs is optimized at the B3LYP and CC2 levels. To avoid bond twists, the excited state structures are assumed to belong to the C_s point group. The structure optimizations of the excited states have been performed using the Karlsruhe SV(P), SVP, TZVP, TZVPP, and aug-TZVPP basis sets; POL12 and PSB12 were not optimized at the aug-TZVPP level. A table containing the minimum and maximum carbon−carbon bond distances as well as the C═N bond lengths is given in Section VII of the SI.

At the B3LYP and MP2 levels, the bond lengths of the ground state structure change by less than 0.2 and 0.3 pm, respectively, when augmenting the TZVP basis set to TZVPP. A similar comparison of the structures obtained using the SVP and TZVP basis sets yields bond length differences that are less than 0.9 and 0.8 pm at the B3LYP and MP2 levels, respectively.

For the first excited state, the structure optimizations at the B3LYP and CC2 levels also yielded very small changes in the bond distances of 0.6 and 0.7 pm, respectively, when augmenting TZVP to TZVPP. The corresponding changes in the bond distances are 0.9 and 1.1 pm when increasing the basis set from SVP to TZVP. For all levels, the bond lengths changed by less than 1 pm when augmenting the TZVPP basis set to aug-TZVPP. Thus, the molecular structures obtained using the TZVPP basis sets are accurate enough for comparisons of the structures obtained with B3LYP or CC2.

The bond lengths obtained in the ground state optimizations at the B3LYP DFT and MP2 levels agree within 1 pm. For the excited state structures, the bond lengths obtained at the B3LYP and CC2 levels agree within 3 pm.

3.4. Bond Length Alternation. Since the pattern for the bond length alternation and the changes in bond lengths upon excitation are similar at the CC2 and DFT levels, the discussion below is valid for both levels. As noted previously for ground state structures of polyenes, the bond length alternation is somewhat sensitive to the amount of exact exchange in the functional.[78]

For the polyenes, the bond lengths change significantly upon excitation. For POL4, the bond length alternation is inverted in the excited state. That is, single bonds become shorter and double bonds longer. For POL6, the bond lengths in the excited state are shorter at the ends of the polyene chain and increase toward the middle. For POL8, POL10, and POL12, the bonds at the ends of the polyenes are shortest, whereas all the other carbon−carbon bonds have almost equal lengths of 140 ± 1 pm. Similar polyene structures were obtained in a recent combined DFT/multi-reference configuration interaction study.[79]

PSBs behave differently. The shortest bond is the C═N bond, whose length is little affected upon excitation. For all PSBs of the present study, the bond length alternation of the ground state is preserved after excitation. The formal single bonds of the ground state remain longer than the

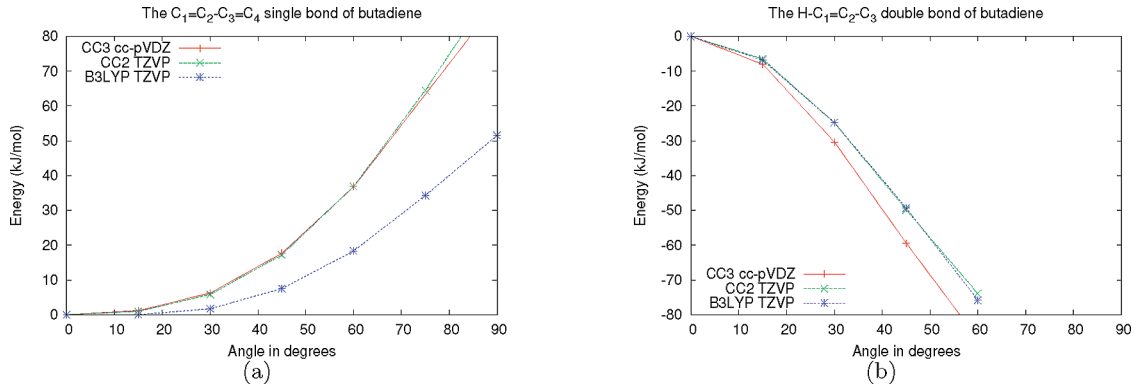

Figure 2. A comparison of potential energy surfaces for torsions of the first excited state of POL4 (*trans*-1,3-butadiene) calculated at different levels of theory. The zero angle corresponds to the planar orientation. (a) The C−C single bond. (b) The C═C double bonds.

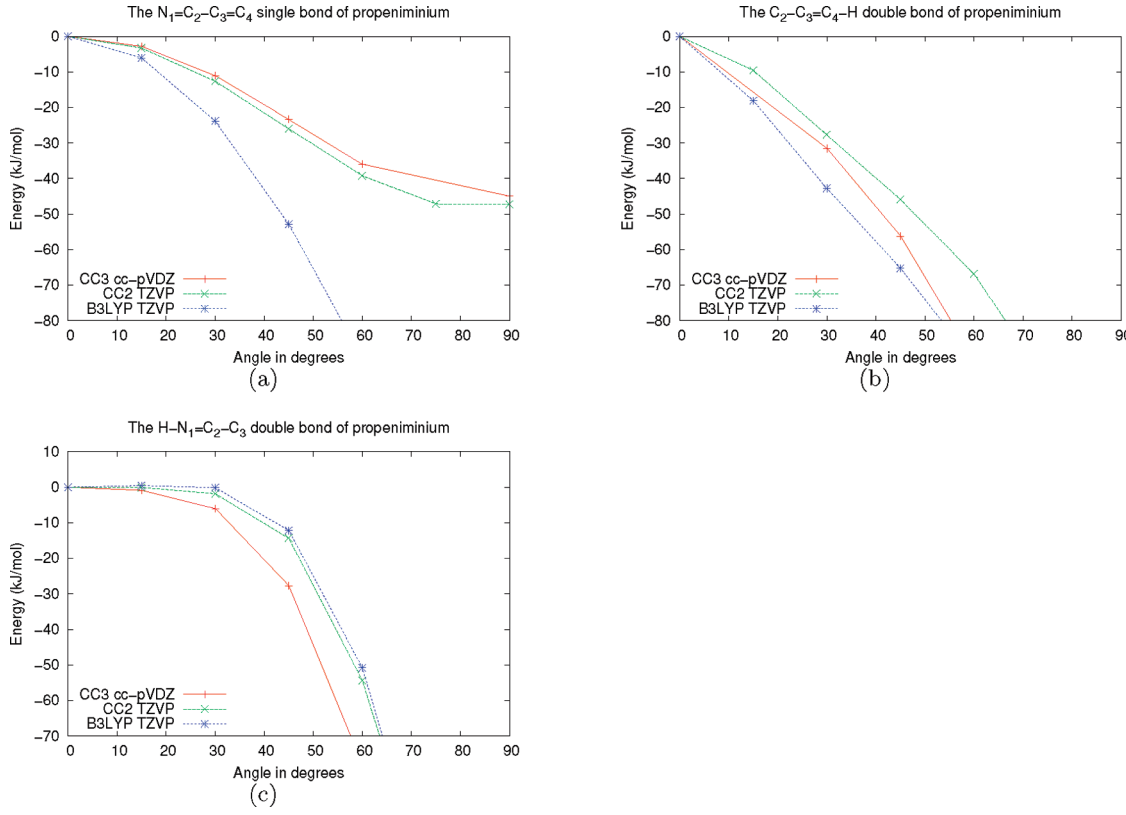

Figure 3. A comparison of the potential energy curves for torsion twists of the carbon−carbon (carbon−nitrogen) bonds for the first excited state of PSB4 (the all-*trans*-2-propeniminium cation) calculated at different levels of theory. The zero angle corresponds to the planar orientation. (a) The C−C single bond. (b) The C═C double bond. (c) The C═N double bond.

formal double bonds. All single bonds extend upon excitation; the C═C double bond at the end shrinks. The other C═C bond lengths remain constant or increase slightly. Compared to the ground state, the bond length alternation is generally enhanced, the effect is more pronounced at the B3LYP level than in the CC2 optimization (see tables in Section VII of the SI).

The different behavior of the polyenes and PSBs can also be seen in the density difference between the ground and excited states for the two classes. As an example, Figure 1 shows the density difference for the untwisted POL6 and PSB6 molecules, for the first excited states of ^1B_u and $^1A'$, respectively. For the polyene, the charge is mainly shifted from the space between atoms, the bonding region, consistent with bond length changes. For the PSB, on the other hand, the charge is mainly shifted from *p*-type orbitals surrounding one atom to another. The exception is the C═C bond most distant from the NH_2^+ group. Here, the charge density is shifted away from the bond region, similarly to what is observed for all C═C bonds in the polyene. With smaller density changes in the bonding region, smaller bond length variations are expected and observed. For PSB6, the electron density in the molecular plane also changes upon excitation, whereas for POL6 only the π density is affected.

For the *cis*-3-pentadieniminium cation, Page and Olivucci found two excited state structures at the CASSCF level, one with inverted and one with enhanced bond length alternation.

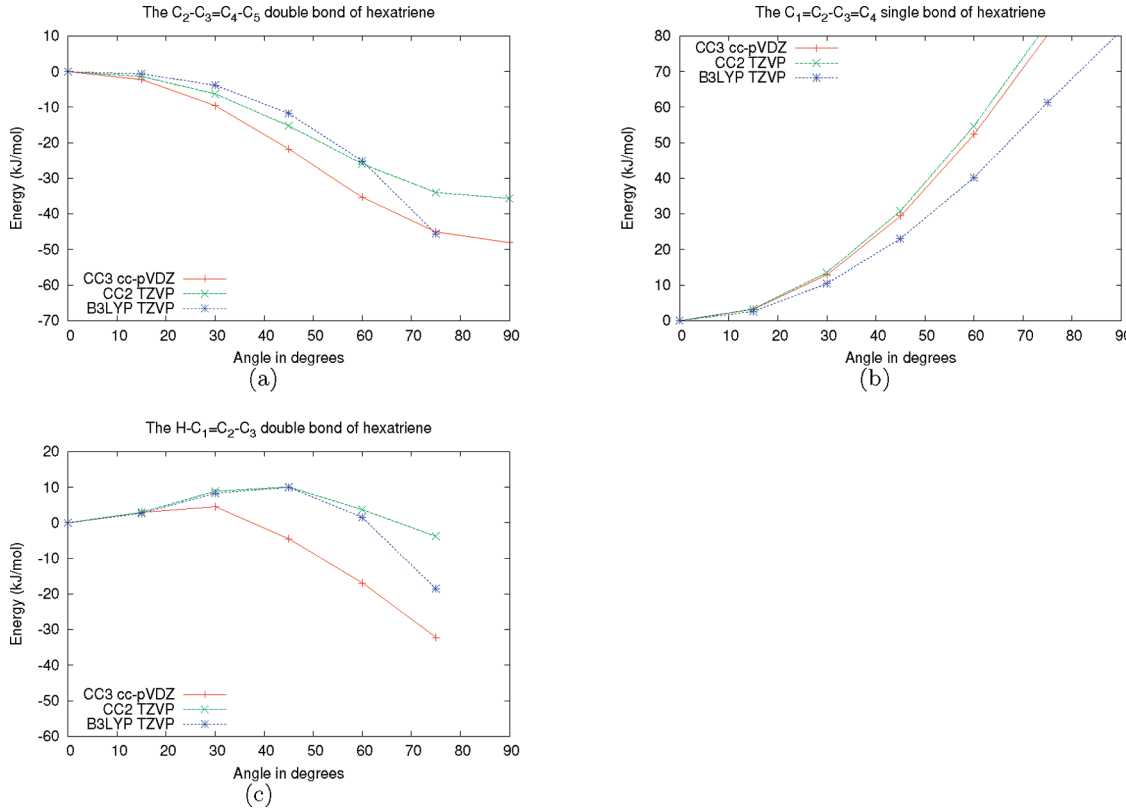

Figure 4. A comparison of the potential energy curves for torsion twists of the carbon−carbon bonds for the first excited state of POL6 (all-*trans*-1,3,5-hexatriene) calculated at different levels of theory. The zero angle corresponds to the planar orientation. (a) The C═C double bond in the middle. (b) The C−C single bonds. (c) The C═C double bonds at both ends.

The CASPT2 optimizations yielded only one minimum with inverted bond length alternation.[27] The present excited state optimizations at the CC2 and B3LYP levels have therefore been repeated using start structures with strongly inverted bond length alternations. These optimizations converged to the same structures as those obtained when starting from the optimized ground state structures. The bond length pattern obtained for excited states of PSBs has been discussed in previous articles and is not addressed in more detail here.[14,80]

4. Effects of Functionals

The PESs of POL6 and PSB6 calculated using different exchange-correlation functionals agree qualitatively. The graphs are given in Section VIII of the SI. The choice of the functional is relevant for torsion barriers when the PES is flat, that is, when the energy remains close to that of the planar structure even for large torsion angles. When the PESs obtained with the various functionals significantly differ, the PESs of the hybrid functionals lie between those of the CAM-B3LYP functional and those of the GGA functionals. Small torsion barriers of less than 5 kJ/mol at the CAM-B3LYP level disappear in the GGA calculations. The PES curve at the C-end of PSB6 calculated at the GGA level has a minimum at a twist of 30°. The potential well vanishes when hybrid functionals are used.

For large torsion angles, the PESs can differ by several tens of kJ/mol. However, strongly twisted structures usually have significant multireference character implying that they are not well described with single-reference methods such as contemporary DFT, which at most can treat mild multireference cases.[81−85] The energies calculated for twisted structures at the TDDFT level therefore become unreliable with increasing torsion angles. In conclusion, the choice of the functional is important when the height of torsion barriers is discussed or PESs remain rather flat.

5. Comparison of B3LYP with CC2 and CC3

5.1. General Trends. For the polyenes, the CC2, CC3, and B3LYP results agree well. The PESs for twists around single bonds are convex and repulsive. For the double-bond twists, they are attractive for POL4 and POL6 and repulsive for POL8, POL10, and POL12. We note that the 1^1B_u state, studied here, is not anymore the lowest excited state for the longer polyenes.

For the PSBs, the situation is much more complicated. No general trends for the PESs are obvious. The PESs have in some cases local minima at a twist of about 30°, and sometimes they have barriers at torsion angles of about 45°. The CC2, CC3, and TDDFT results are in qualitative agreement for most of the bonds. Exceptions are single-bond twists of PSB6, PSB8, PSB10, and PSB12, mainly where the PES is essentially flat at the CC2 level. The agreement between the TDDFT level and the two coupled cluster (CC) levels is better for double-bond twists than for single-bond twists. For small deviations from the planar structure, the PESs of the B3LYP calculations are in very close agreement with those obtained at the CC levels. The comparison of CC2 and CC3 results shows that triple excitations are more

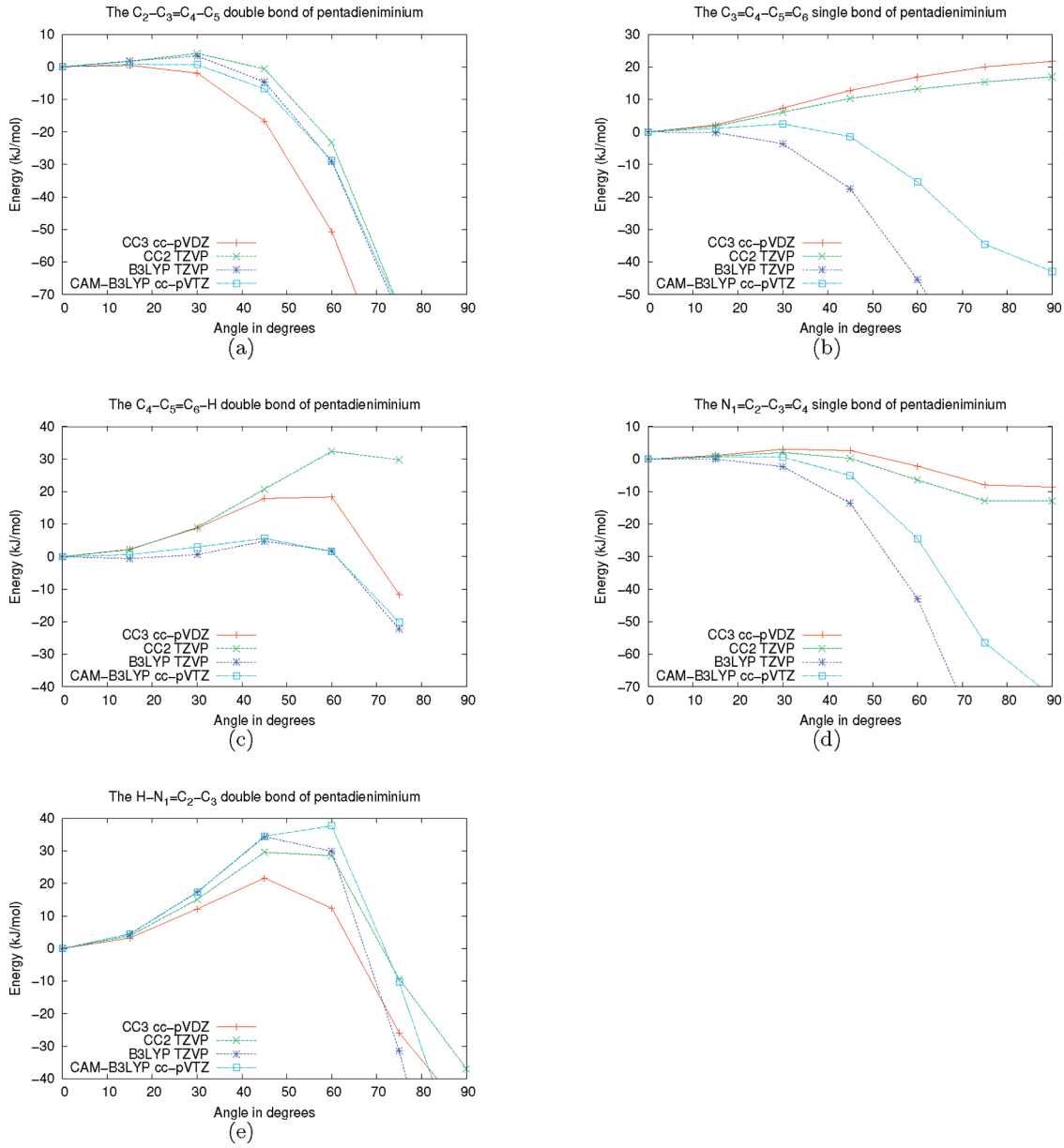

Figure 5. A comparison of the potential energy curves for torsion twists of the carbon−carbon (carbon−nitrogen) bonds for the first excited state of PSB6 (the all-*trans*-2,4-pentadieniminium cation) calculated at different levels of theory. The zero angle corresponds to the planar orientation. (a) The C=C double bond in the middle. (b) The C−C bond closer to the carbon end. (c) The C=C bond at the carbon end. (d) The C−C bond closer to the nitrogen end. (e) The C=N double bond.

important for double-bond twists than for single-bond twists, as expected.

To investigate the effect of the Franck−Condon relaxation on the torsion barriers, the molecular structures of the excited states are optimized, assuming that the molecules belong to the C_s point group. The calculations of the PESs for the bond twists yield similar curves as obtained when the ground state structures are used as starting geometry. The studied molecules have large torsion barriers for all bonds in the ground state. The ground state PESs and the excited state PESs for POL6 and PSB6 are given in Section VIII of the SI.

In the following, we discuss only the molecules of chain length 4, 6, and 8 in detail. The data for molecules of chain length 10 and 12 are given in Section X of the SI.

5.2. POL4 and PSB4. The PESs for the single- and double-bond twists of the first excited state of POL4 and PSB4 are shown in Figures 2 and 3. The PES for the single-bond twist of POL4 is convex and repulsive, whereas for the double-bond twist it is concave and attractive. The PESs for the torsion twists of all the PSB4 bonds are attractive and concave. PSB4 has no torsion barriers for bond twists in the first excited state. The calculations at the B3LYP, CC2, and CC3 levels yield qualitatively similar PESs. The largest differences are obtained for the single bonds. The torsion barrier for the single-bond twist of POL4 is lowest at the B3LYP level. For PSB4, the PES of the single-bond twist falls steeper at the B3LYP level than at the CC level.

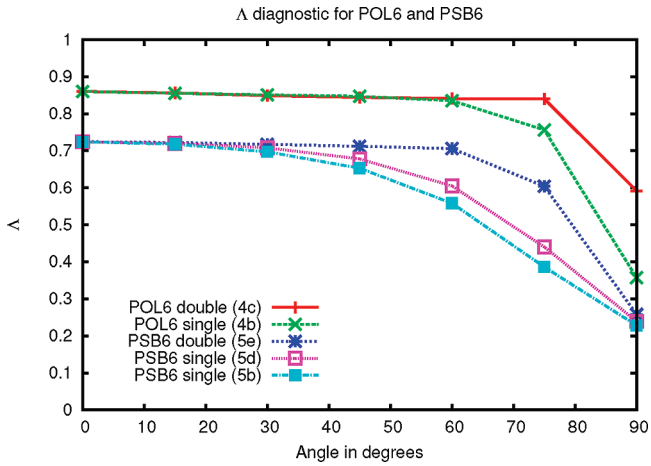

Figure 6. The Λ-diagnostic values for twists around selected single and double bonds of POL6 and PSB6, calculated at the B3LYP/TZVP level. The corresponding figures for the potential energy surfaces are indicated within parentheses.

5.3. POL6 and PSB6. The PESs for the single- and double-bond twists of POL6 and PSB6 are shown in Figures 4 and 5. For POL6, the double-bond twists are attractive. The PES of the double bond at the polyene end is convex yielding a small barrier of 5−10 kJ/mol depending on the computational level.

For the PSB6 double-bond twists, the PESs are attractive and convex except for the double bond in the middle of the molecule at the CC3 level. The small barrier of less than 5 kJ/mol for the mid C═C bond, obtained at the B3LYP and CC2 levels, is probably due to missing higher order correlation effects. The two other double bonds have barrier maxima at around 60°. The torsion barrier for the C═C bond at the end is larger at the CC levels than at the B3LYP level. The lowest C═N torsion barrier of about 20 kJ/mol is obtained at the CC3 level. For the double bonds, the B3LYP and CAM-B3LYP calculations yielded very similar PESs, indicating that the charge transfer problem does not significantly affect these PESs. The charge density differences upon excitation confirm this view, see Figure 1.

For the PSB6 single-bond twists, the PESs obtained at the CC and B3LYP levels do not completely agree. For the single bond at the N-end, all methods give attractive PESs. The CC and CAM-B3LYP calculations yield convex PESs with a tiny barrier of 0.7−3.0 kJ/mol, whereas the B3LYP calculations yield a concave PES. The coupled cluster PES is flat with the energy of the perpendicular structure less than 15 kJ/mol below that of the planar one. The PESs calculated at the TDDFT level are attractive, barrierless, and steep. For the single bond at the C-end, the CC curves are convex, essentially flat, but repulsive. The energy for the perpendicular structure is about 20 kJ/mol above that for the planar one. Opposed to this, the TDDFT curves are steep and attractive. The PES is barrierless at the B3LYP level but has a 2.5 kJ/mol barrier at the CAM-B3LYP level. For the longer PSBs, similar discrepancies are obtained between the PESs at the CC2 and B3LYP levels.

The CAM-B3LYP functional has been introduced to improve the performance of the TDDFT approach for charge transfer excitations. For the single-bond twists where the PESs calculated at the B3LYP level do not reproduce the CC ones, the CAM-B3LYP calculations yield PESs lying between the B3LYP and the CC ones. However, the CAM-B3LYP curves agree better with the B3LYP ones than with the CC curves. This indicates that nonlocal charge transfer might contribute but does not explain the difficulties of the TDDFT method to provide accurate PESs for single-bond twists of the PSBs. This is also seen in the comparison of the PESs calculated with various functionals given in Section VIII of the SI.

The PESs show that the TDDFT problem to describe the energy surfaces of the single-bond twists can in this case not be reduced only to the charge transfer issue. This is further confirmed by the Λ-diagnostic recently proposed by Peach et al.[86] Λ is a measure of the orbital overlap between the occupied and virtual orbitals involved in the excitation and is between zero and one; a higher value corresponds to a more local excitation. Excitations with a small Λ value were proposed to be badly described by standard GGAs and hybrid functionals.[86]

Figure 6 shows how Λ varies with torsion angle for selected double and single bonds for POL6 and PSB6. For the double bonds as well as the POL6 single bond Λ is quite high, even for angles approaching 90 degrees. For these twists, the TDDFT methods also compare well with the coupled cluster results. The troublesome single bond twists of PSB6 behave differently. With increasing twist angle, Λ falls off sooner than for the other bonds. A correlation between increasing error and a decreasing Λ value can be noted. The deviation between DFT and CC kicks in much before the diagnostic falls below the suggested critical value of $\Lambda < 0.4$,[86] however. Thus, the Λ diagnostic indicates no severe charge-transfer issue.

5.4. POL8 and PSB8. The PESs for POL8 and PSB8 calculated at the B3LYP and CC2 levels are shown in Figure 7. For POL8, the PESs for all double-bond twists are convex with the barrier maximum at 45−60°. For large angles, significant differences between the CC2 and B3LYP curves appear. However, the multiconfiguration character of the wave function is large for structures with perpendicular bond orientation, again implying that the PESs are unreliable at large torsion angles. The PESs for the double-bond twists of PSB8 calculated at the CC2 and B3LYP levels agree better than for POL8. The smallest double-bond torsion barrier for PSB8 of 20 kJ/mol is obtained for the C═C double bond closer to the C═N end. The corresponding C═C double bond for POL8 has a torsion barrier of 10 kJ/mol. The torsion barriers for the other double bonds are also higher for PSB8 than for POL8.

For the single-bond twists of POL8, the PESs calculated at the CC2 and B3LYP levels agree well, whereas significant differences are obtained for PSB8. For the single bond at the N-end and in the middle, the CC2 curves are convex and repulsive but flat. For these two single bonds, the B3LYP calculations yield convex and attractive PESs. The torsion barrier for the single bond at the N-end

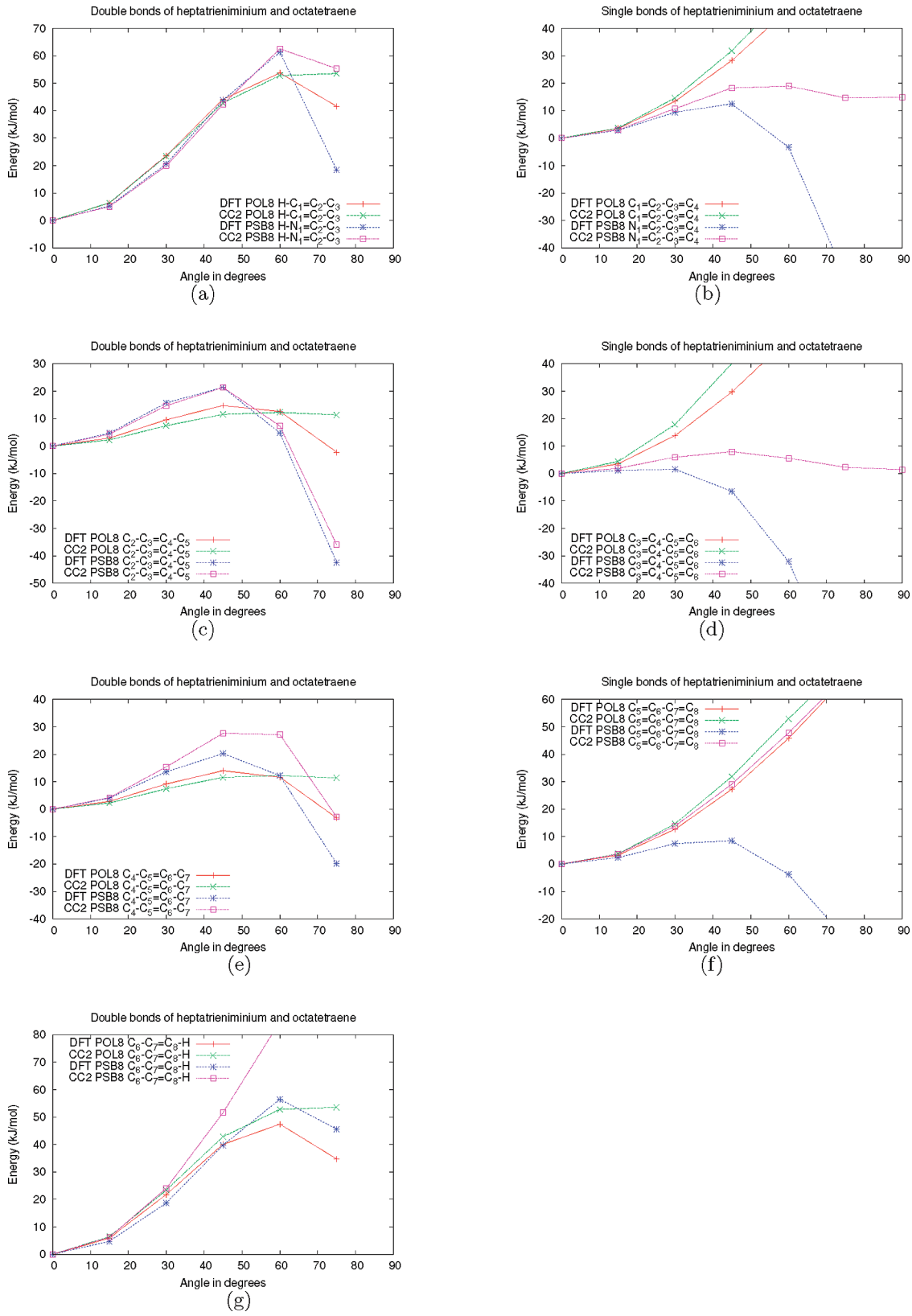

Figure 7. A comparison of the torsion barriers of the single and double bonds of POL8 (all-*trans*-1,3,5,7-octatetraene) and PSB8 (the all-*trans*-2,4,6-heptatrieniminium cation) calculated at the B3LYP TDDFT and CC2 levels. (a) The $C_1{=}C_2$ ($N_1{=}C_2$) bond, (b) $C_2{-}C_3$, (c) $C_3{=}C_4$, (d) $C_4{-}C_5$, (e) $C_5{=}C_6$, (f) $C_6{-}C_7$, and (g) the $C_7{=}C_8$ bond.

is less than 15 kJ/mol and almost vanishes for the single bond in the middle. The CC2 curve for the single bond at the C-end of PSB8 is convex and strongly repulsive, whereas the B3LYP curve is convex and strongly attractive leading to a torsion barrier of about 10 kJ/mol. In this case, the B3LYP calculations fail to reproduce the main trends of the PESs calculated at the CC2 level, in contrast to the two other single bonds.

The PESs of POL10, PSB10, POL12, and PSB12 are similar to those of their shorter homologues, POL8 and PSB8. The agreement of the CC2 and B3LYP levels is generally better than for POL8 and PSB8. The PESs for all bond torsions can be found in Section X of the SI.

6. Conclusion and Summary

Systematic studies of the potential energy surfaces (PESs) for the torsion twists of the first excited state of polyenes and PSBs, with chain lengths of 4−12 heavy atoms, revealed a remarkably different behavior of the two compound groups. While the excited states of the polyenes exhibit high torsion barriers for single-bond twists, the PSBs have low or vanishing torsion barriers for both single- and double-bond twists. PSBs are very flexible molecules in the first excited state, and most of the bonds are likely to contribute to the excited state dynamics, whereas in polyenes the dynamics are limited to motions around double bonds. The flexibility of PSBs in the excited state and the thermal ground state flexibility of 11-*cis*-retinal[87] are typical for the complexity of the retinal photoisomerisation.

Benchmark calculations of the excitation energies show that diffuse functions must be included in the basis set to reach the basis set limit of the polyenes, whereas diffuse functions are less important for the lowest states of the cationic PSBs. For an accurate description of the potential energy surfaces of the polyenes and PSBs, diffuse basis functions are not mandatory, due to cancellation of errors in the excitation energies.

Exchange-correlation functional studies at the TDDFT level employing GGA, hybrid, and Coulomb-attenuated functionals yield similar PESs. The PESs obtained with hybrid functionals lie in between those calculated at the GGA values on the one side and the CAM-B3LYP values on the other side. The influence of the functional is important when the potential barriers or wells are very flat.

Comparisons of the calculated excitation energies and PESs for the polyenes and the corresponding PSBs indicate that CC2 calculations are useful for retinal studies. The obtained PESs are in close agreement with those calculated at the CC3 level, where triple excitations are taken into account. The single-bond torsion barriers obtained at the CC2 and CC3 levels are in excellent agreement, whereas for the double-bond twists, CC2 gives somewhat higher barriers than CC3. The differences between the PESs obtained at the two CC levels are, however, small.

Comparison of the DFT and CC calculations shows that the PESs agree well for double-bond twists, whereas significant differences are found for the single-bond torsions of the longer PSBs. The low or vanishing barriers for torsions around the single bond farthest away from the C=N moiety are apparently a flaw of the TDDFT method. The TDDFT results are only slightly improved by using the CAM-B3LYP functional in those cases where calculations at the B3LYP level fail to reproduce the CC2 results. The TDDFT problems are not merely due to the inability to describe long-range charge transfer effects. TDDFT performs well for the polyenes and for PSB double-bond twists. In TDDFT studies on the 11-*cis* retinal PSB, the largest difference between the PESs obtained at the TDDFT and CC2 level appears at the bond connecting the retinyl chain with the β-ionone ring. In the first excited state, TDDFT optimizations yield a perpendicular orientation of the β-ionone-ring plane with respect to the retinyl-chain plain.[38] Single-bond twists of longer PSBs show that the TDDFT results are satisfactory for small torsion angles. We conclude that even though TDDFT might suffer from long-range charge transfer problems and that it apparently provides incorrect PESs at large torsion angles, one should not exclude it from the toolbox of retinal studies. However, it is necessary to confirm excited state TDDFT studies on retinal PSBs by performing calculations at *ab initio* correlation levels such as CC2.

Acknowledgment. This research has been supported by the Academy of Finland through its Centers of Excellence Programme 2006−2011, the OPNA research project (118195), the Centre for Functional Nanostructures (CFN) of the Deutsche Forschungsgemeinschaft (DFG) within project C3.9, the Lundbeck Foundation, and the Foundation for Polish Science (FNP) (Homing program grant no. HOM/2008/10B) within the EEA Financial Mechanism. The research collaboration is supported by the Nordic Centre of Excellence in Computational Chemistry (NCoECC) project funded by NordForsk (070253). We also thank CSC - the Finnish IT Center for Science and the Danish Center for Scientific Computing (DCSC) for computer time. We are grateful to Prof. Reinhart Ahlrichs for helpful discussions.

Supporting Information Available: Optimized Cartesian coordinates for ground and excited states (in C_s symmetry) including C−C and C−N distances; structures and systematic chemical names of the studied molecules; basis set studies of the potential energy surfaces at the CC2, CC3, and B3LYP levels; potential energy surfaces studied using different exchange-correlation functionals; potential energy curves for the double-bond twists of PSB10, POL10, PSB12, and POL12; $\mathcal{T}_1$ diagnostic values. This material is available free of charge via the Internet at http://pubs.acs.org.

References

(1) Shichida, Y.; Kobayashi, T.; Ohtani, H.; Yoshizawa, T.; Nagakura, S. Picosecond Laser Photolysis of Squid Rhodopsin at Room and Low Temperatures. *Photochem. Photobiol.* **1978**, *27*, 335–341.

(2) Yoshizawa, T.; Shichida, Y.; Matuoka, S. Primary intermediates of rhodopsin studied by low temperature spectrophotometry and laser photolysis: Bathorhodopsin, hypsorhodopsin and photorhodopsin. *Vision Res.* **1984**, *24*, 1455–1463.

(3) Shichida, Y.; Matuoka, S.; Yoshizawa, T. Formation of photorhodopsin, a precursor of bathorhodopsin, detected by a picosecond laser photolysis at room temperature. *Photobiochem. Photobiophys.* **1984**, *7*, 221–228.

(4) Schoenlein, R. W.; Peteanu, L. A.; Mathies, R. A.; Shank, C. V. The 1st Step in Vision - Femtosecond Isomerization of Rhodopsin. *Science* **1991**, *254*, 412–415.

(5) Kandori, H.; Shichida, Y.; Yoshizawa, T. Photoisomerization in Rhodopsin. *Biochemistry (Moscow)* **2001**, *66*, 1197–1209.

(6) Okada, T.; Ernst, O. P.; Palczewski, K.; Hoffmann, K. P. Activation of rhodopsin: new insights from structural and biochemical studies. *Trends Biochem. Sci.* **2001**, *26*, 318–324.

(7) Schreiber, M.; Sugihara, M.; Okada, T.; Buss, V. Quantum Mechanical Studies on the Crystallographic Model of Bathorhodopsin. *Angew. Chem., Int. Ed.* **2006**, *45*, 4274–4277.

(8) Nakamichi, H.; Okada, T. Crystallographic Analysis of Primary Visual Photochemistry. *Angew. Chem., Int. Ed.* **2006**, *45*, 4270–4273.

(9) Kukura, P.; McCamant, D. W.; Yoon, S.; Wandschneider, D. B.; Mathies, R. A. Structural Observation of the Primary Isomerization in Vision with Femtosecond-Stimulated Raman. *Science* **2005**, *310*, 1006–1009.

(10) Yoshizawa, T.; Wald, G. Pre-Lumirhodopsin and the Bleaching of Visual Pigments. *Nature* **1963**, *197*, 1279–1286.

(11) Vreven, T.; Bernardi, F.; Garavelli, M.; Olivucci, M.; Robb, M. A.; Schlegel, H. B. Ab Initio Photoisomerization Dynamics of a Simple Retinal Chromophore Model. *J. Am. Chem. Soc.* **1997**, *119*, 12687–12688.

(12) Garavelli, M.; Celani, P.; Bernardi, F.; Robb, M. A.; Olivucci, M. The $C_5H_6NH_2^+$ Protonated Shiff Base: An ab Initio Minimal Model for Retinal Photoisomerization. *J. Am. Chem. Soc.* **1997**, *119*, 6891–6901.

(13) Garavelli, M.; Vreven, T.; Celani, P.; Bernardi, F.; Robb, M. A.; Olivucci, M. Photoisomerization Path for a Realistic Retinal Chromophore Model: Nonatetraeniminimum Cation. *J. Am. Chem. Soc.* **1998**, *120*, 1285–1288.

(14) Aquino, A. J. A.; Barbatti, M.; Lischka, H. Excited-State Properties and Environmental Effects for Protonated Schiff Bases: A Theoretical Study. *Chem. Phys. Chem.* **2006**, *7*, 2089–2096.

(15) Barbatti, M.; Granucci, G.; Persico, M.; Ruckenbauer, M.; Vazdar, M.; Eckert-Maksić, M.; Lischka, H. The on-the-fly surface-hopping program system Newton-X: Application to ab initio simulation of the nonadiabatic photodynamics of benchmark systems. *J. Photochem. Photobiol. A: Chem.* **2007**, *190*, 228–240.

(16) Szymczak, J. J.; Barbatti, M.; Lischka, H. Mechanism of Ultrafast Photodecay in Restricted Motions in Protonated Schiff Bases: The Pentadieniminium Cation. *J. Chem. Theory Comput.* **2008**, *4*, 1189–1199.

(17) Roos, B. O.; Taylor, P. R. A Complete Active Space SCF Method (CASSCF) using a Density-Matrix Formulated Super-CI Approach. *Chem. Phys.* **1980**, *48*, 157–173.

(18) Andersson, K.; Malmqvist, P. Å.; Roos, B. O. 2nd-order perturbation-theory with a complete active space self-consistent field reference function. *J. Chem. Phys.* **1992**, *96*, 1218–1226.

(19) Olsen, J.; Roos, B. O.; Jørgensen, P.; Jensen, H. J. A. Determinant Based Configuration-Interaction Algorithms for Complete and Restricted Configuration-Interaction Spaces. *J. Chem. Phys.* **1988**, *89*, 2185–2192.

(20) Malmqvist, P. Å.; Pierloot, K.; Shahi, A. R. M.; Cramer, C. J.; Gagliardi, L. The restricted active space followed by second-order perturbation theory method: Theory and application to the study of CuO_2 and Cu_2O_2 systems. *J. Chem. Phys.* **2008**, *128*, 204109.

(21) Altun, A.; Yokoyama, S.; Morokuma, K. Mechanism of Spectral Tuning Going from Retinal in Vacuo to Bovine Rhodopsin and its Mutants: Multireference ab Initio Quantum Mechanics/Molecular Mechanics Studies. *J. Phys. Chem. B* **2008**, *112*, 16883–16890.

(22) Cembran, A.; González-Luque, R.; Altoè, P.; Merchán, M.; Bernardi, F.; Olivucci, M.; Garavelli, M. Structure, Spectroscopy, and Spectral Tuning of the Gas-Phase Retinal Chromophore: The β-Ionone "Handle" and the Alkyl Group Effect. *J. Phys. Chem. A* **2005**, *109*, 6597–6605.

(23) Cembran, A.; Bernardi, F.; Olivucci, M.; Garavelli, M. The retinal chromophore/chloride ion pair: Structure of the photoisomerization path and interplay of charge transfer and covalent states. *Proc. Natl. Acad. Sci. U.S.A.* **2005**, *102*, 6255–6260.

(24) González-Luque, R.; Garavelli, M.; Bernardi, F.; Merchán, M.; Robb, M. A.; Olivucci, M. Computational evidence in favor of a two-state, two-mode model of the retinal chromophore potoisomerization. *Proc. Natl. Acad. Sci. U.S.A.* **2000**, *92*, 9379–9384.

(25) Sekharan, S.; Weingart, O.; Buss, V. Ground and Excited States of Retinal Schiff Base Chromophores by Multiconfigurational Perturbation Theory. *Biophys. J.* **2006**, *91*, L07–L09.

(26) Johansson, M. P.; Olsen, J. Torsional Barriers and Equilibrium Angle of Biphenyl: Reconciling Theory with Experiment. *J. Chem. Theory Comput.* **2008**, *4*, 1460–1471.

(27) Page, C. S.; Olivucci, M. Ground and Excited State CASPT2 Geometry Optimizations of Small Organic Molecules. *J. Comput. Chem.* **2003**, *24*, 298–309.

(28) Gross, E. K. U.; Kohn, W. Time-dependent density functional theory. *Adv. Quantum Chem.* **1990**, *21*, 255–291.

(29) Bauernschmitt, R.; Ahlrichs, R. Treatment of electronic excitations within the adiabatic approximation of time dependent density functional theory. *Chem. Phys. Lett.* **1996**, *256*, 454–464.

(30) van Leeuwen, R. Key concepts in time-dependent density-functional theory. *Int. J. Mod. Phys. B* **2001**, *15*, 1969–2023.

(31) Furche, F.; Burke, K. Time-dependent density functional theory in quantum chemistry. In *Annual Reports in Computational Chemistry, 1*; Spellmeyer, D., Ed.; Elsevier: Amsterdam, 2005; pp 19−30.

(32) Burke, K.; Werschnick, J.; Gross, E. K. U. Time-dependent density functional theory: Past, present, and future. *J. Chem. Phys.* **2005**, *123*, 062206.

(33) Furche, F.; Ahlrichs, R. Adiabatic time-dependent density functional methods for excited state properties. *J. Chem. Phys.* **2002**, *117*, 7433–7447.

(34) Maitra, N. T.; Zhang, F.; Cave, R. J.; Burke, K. Double excitations within time-dependent density functional theory linear response. *J. Chem. Phys.* **2004**, *120*, 5932–5937.

(35) Cave, R. J.; Zhang, F.; Maitra, N. T.; Burke, K. A dressed TDDFT treatment of the 2^1A_g states of butadiene and hexatriene. *Chem. Phys. Lett.* **2004**, *389*, 39–42.

(36) Mikhailov, I. A.; Tafur, S.; Masunov, A. E. Double excitations and state-to-state transition dipoles in π-π^* excited singlet states of linear polyenes: Time-dependent density-functional theory versus multiconfigurational methods. *Phys. Rev. A* **2008**, *77*, 012510.

(37) Mazur, G.; Włodarczyk, R. Application of the Dressed Time-Dependent Density Functional Theory for the Excited States of Linear Polyenes. *J. Comput. Chem.* **2009**, *30*, 811–817.

(38) Send, R.; Sundholm, D. The role of the β-ionone ring in the photochemical reaction of rhodopsin. *J. Phys. Chem. A* **2007**, *111*, 27–33.

(39) Send, R.; Sundholm, D. Coupled-Cluster Studies of the Lowest Excited States of the 11-cis-Retinal Chromophore. *Phys. Chem. Chem. Phys.* **2007**, *9*, 2862–2867.

(40) Send, R.; Sundholm, D. Stairway to the Conical Intersection: A Computational Study of the Retinal Isomerization. *J. Phys. Chem. A* **2007**, *111*, 8766–8773.

(41) Send, R.; Sundholm, D. The molecular structure of a curl-shaped retinal isomer. *J. Mol. Model.* **2008**, *14*, 717–726.

(42) Wanko, M.; Garavelli, M.; Bernardi, F.; Miehaus, T. A.; Frauenheim, T.; Elstner, M. A global investigation of excited state surfaces within time-dependent density-functional response theory. *J. Chem. Phys.* **2004**, *120*, 1674–1692.

(43) Dreuw, A.; Head-Gordon, M. Single-Reference ab initio Methods for the Calculation of Excited States of Large Molecules. *Chem. Rev.* **2005**, *105*, 4009–4037.

(44) Christiansen, O.; Koch, H.; Jørgensen, P. The 2nd-order Approximate Coupled-Cluster Singles and Doubles Model CC2. *Chem. Phys. Lett.* **1995**, *243*, 409–418.

(45) Hättig, C.; Weigend, F. CC2 excitation energy calculations on large molecules using the resolution of the identity approximation. *J. Chem. Phys.* **2000**, *113*, 5154–5161.

(46) Nielsen, I. B.; Lammich, L.; Andersen, L. H. S_1 and S_2 excited states of gas-phase Schiff-base retinal chromophores. *Phys. Rev. Lett.* **2006**, *96*, 018304.

(47) Koch, H.; Christiansen, O.; Jørgensen, P.; Sanchez de Merás, A. M.; Helgaker, T. The CC3 model: An iterative coupled cluster approach including connected triples. *J. Chem. Phys.* **1997**, *106*, 1808–1818.

(48) Pescitelli, G.; Sreerama, N.; Salvadori, P.; Nakanishi, K.; Berova, N.; Woody, R. W. Inherent Chirality Dominates the Visible/Near-Ultraviolet CD Spectrum of Rhodopsin. *J. Am. Chem. Soc.* **2008**, *130*, 6170–6181.

(49) Zaari, R. R.; Wong, S. Y. Y. Photoexcitation of 11-Z-cis-7,8-dihydro retinal and 11-Z-cis retinal: A comparative computational study. *Chem. Phys. Lett.* **2009**, *469*, 224–228.

(50) Chmura, B.; Rode, M. F.; Sobolewski, A. L.; Lapinski, L.; Nowak, M. J. A Computational Study on the Mechanism of Intramolecular Oxo-Hydroxy Phototautomeris Driven by Repulsive $\pi\sigma^*$ State. *J. Phys. Chem. A* **2008**, *112*, 13655–13661.

(51) Rode, M. F.; Sobolewski, A. L.; Dedonder, C.; Jouvet, C.; Dopfer, O. Computational Study on the Photophysics of Protonated Benzene. *J. Phys. Chem. A* **2009**, *113*, 5865–5873.

(52) Dunning, T. H., Jr. Gaussian basis sets for use in correlated molecular calculations. I. The atoms boron through neon and hydrogen. *J. Chem. Phys.* **1989**, *90*, 1007–1023.

(53) Peterson, K. A.; Woon, D. E.; Dunning, T. H., Jr. Benchmark calculations with correlated molecular wave functions. IV. The classical barrier height of the $H+H_2 \rightarrow H_2+H$ reaction. *J. Chem. Phys.* **1994**, *100*, 7410–7415.

(54) Wilson, A.; van Mourik, T.; Dunning, T. H., Jr. Gaussian basis sets for use in correlated molecular calculations. VI. Sextuple zeta correlation consistent basis sets for boron through neon. *J. Mol. Struct. (Theochem)* **1997**, *388*, 339–349.

(55) Becke, A. D. Density-functional thermochemistry. III. The role of exact exchange. *J. Chem. Phys.* **1993**, *98*, 5648–5652.

(56) Lee, C.; Yang, W.; Parr, R. G. Development of the Colle-Salvetti correlation-energy formula into a functional of the electron density. *Phys. Rev. B* **1988**, *37*, 785–789.

(57) Schäfer, A.; Horn, H.; Ahlrichs, R. Fully Optimized Contracted Gaussian-Basis Sets for Atoms Li to Kr. *J. Chem. Phys.* **1992**, *97*, 2571–2577.

(58) Schäfer, A.; Huber, C.; Ahlrichs, R. Fully Optimized Contracted Gaussian-Basis Sets of Triple Zeta Valence Quality for Atoms Li to Kr. *J. Chem. Phys.* **1994**, *100*, 5829–5835.

(59) Weigend, F.; Häser, M.; Patzelt, H.; Ahlrichs, R. RI-MP2: optimized auxiliary basis sets and demonstration of efficiency. *Chem. Phys. Lett.* **1998**, *294*, 143–152.

(60) Weigend, F.; Ahlrichs, R. Balanced basis sets of split valence, triple zeta valence and quadruple zeta valence quality for H to Rn: Design and assessment of accuracy. *Phys. Chem. Chem. Phys.* **2005**, *7*, 3297–3305.

(61) Vosko, S. H.; Wilk, L.; Nusair, M. Accurate Spin-Dependent Electron Liquid Correlation Energies for Local Spin-Density Calculations - a Critical Analysis. *Can. J. Phys.* **1980**, *58*, 1200–1211.

(62) Perdew, J. P. Density-functional approximation for the correlation energy of the inhomogeneous electron gas. *Phys. Rev. B* **1986**, *33*, 8822–8824.

(63) Becke, A. D. Density-functional exchange-energy approximation with correct asymptotic behavior. *Phys. Rev. A* **1988**, *38*, 3098–3100.

(64) Perdew, J. P.; Burke, K.; Ernzerhof, M. *Phys. Rev. Lett.* **1996**, *77*, 3865–3868.

(65) Perdew, J. P.; Burke, K.; Ernzerhof, M. Rationale for mixing exact exchange with density functional approximations. *J. Chem. Phys.* **1996**, *105*, 9982–9985.

(66) Yanai, T.; Tew, D. P.; Handy, N. C. A new hybrid exchange-correlation functional using the Coulomb-attenuating method (CAM-B3LYP). *Chem. Phys. Lett.* **2004**, *393*, 51–57.

(67) Møller, C.; Plesset, M. S. Note on an Approximation Treatment for Many-Electron Systems. *Phys. Rev.* **1934**, *46*, 618–622.

(68) Feyereisen, M.; Fitzgerald, G.; Komornicki, A. Use of approximate integrals in ab initio theory. An application in MP2 energy calculations. *Chem. Phys. Lett.* **1993**, *208*, 359–363.

(69) Weigend, F.; Häser, M. RI-MP2: first derivatives and global consistency. *Theor. Chem. Acc.* **1997**, *97*, 331–340.

(70) Christiansen, O.; Koch, H.; Jørgensen, P. Perturbative triple excitation corrections to coupled cluster singles and doubles excitation energies. *J. Chem. Phys.* **1996**, *105*, 1451–1459.

(71) Hald, K.; Jorgensen, P.; Olsen, J.; Jaszuñski, M. An analysis and implementation of a general coupled cluster approach to excitation energies with application to the B_2 molecule. *J. Chem. Phys.* **2001**, *115*, 671–679.

(72) Dalton, an ab initio electronic structure program, Release 2.0; 2005. See http://www.kjemi.uio.no/software/dalton/dalton.html (accessed month day, year).

(73) Ahlrichs, R.; Bär, M.; Häser, M.; Horn, H.; Kölmel, C. Electronic Structure Calculations on Workstation Computers: The Program System TURBOMOLE. *Chem. Phys. Lett.* **1989**, *162*, 165–169. Current version. See http://www.turbomole.com (accessed month day, year).

(74) Laaksonen, L. A graphics program for the analysis and display of molecular dynamics trajectories. *J. Mol. Graph.* **1992**, *10*, 33–34.

(75) Bergman, D. L.; Laaksonen, L.; Laaksonen, A. Visualization of solvation structures in liquid mixtures. *J. Mol. Graphics Modell.* **1997**, *15*, 301–306.

(76) Lehtonen, O.; Sundholm, D.; Send, R.; Johansson, M. P. Density Functional Theory and Coupled-Cluster Studies of the Electronic Excitation Spectra of trans-1,3-butadiene and trans-2-propeniminium. *J. Chem. Phys.* **2009**, *131*, 024301.

(77) Lee, T. J.; Taylor, P. R. A Diagnostic for Determining the Quality of Single-Reference Electron Correlation Methods. *Int. J. Quant. Chem. Symp.* **1989**, *23*, 199–207.

(78) Peach, M. J. G.; Tellgren, E. I.; Sałek, P.; Helgaker, T.; Tozer, D. J. Structural and Electronic Properties of Polyacetylene and Polyyne from Hybrid and Coulomb-Attenuated Density Functionals. *J. Phys. Chem. A* **2007**, *111*, 11930–11935.

(79) Marian, C. M.; Gilka, N. Performance of the Density Functional Theory/Multireference Configuration Interaction Method on Electronic Excitation of Extended π-Systems. *J. Chem. Theory Comput.* **2008**, *4*, 1501–1515.

(80) Tavernelli, I.; Röhrig, U. F.; Rothlisberger, U. Molecular dynamics in electronically excited states using time-dependent density functional theory. *Mol. Phys.* **2005**, *103*, 963–981.

(81) Handy, N. C.; Cohen, A. J. Left-right correlation energy. *Mol. Phys.* **2001**, *99*, 403–412.

(82) Polo, V.; Kraka, E.; Cremer, D. Electron correlation and the self-interaction error of density functional theory. *Mol. Phys.* **2002**, *100*, 1771–1790.

(83) Polo, V.; Kraka, E.; Cremer, D. Some thoughts about the stability and reliability of commonly used exchange-correlation functionals - coverage of dynamic and nondynamic correlation effects. *Theor. Chem. Acc.* **2002**, *107*, 291–303.

(84) Cremer, D.; Filatov, M.; Polo, V.; Kraka, E.; Shaik, S. Implicit and Explicit Coverage of Multi-reference Effects by Density Functional Theory. *Int. J. Mol. Sci.* **2002**, *3*, 604–638.

(85) Johansson, M. P.; Sundholm, D. Spin and charge distribution in iron porphyrin models: A coupled cluster and density-functional study. *J. Chem. Phys.* **2004**, *120*, 3229–3236.

(86) Peach, M. J. G.; Benfield, P.; Helgaker, T.; Tozer, D. J. Excitation energies in density functional theory: An evaluation and a diagnostic test. *J. Chem. Phys.* **2008**, *128*, 044118.

(87) Silva López, C.; Álvarez, R.; Domínguez, M.; Nieto Faza, O.; de Lera, Á. R. Complex Thermal Behavior of 11-cis-Retinal, the Ligand of Visual Pigments. *J. Org. Chem.* **2009**, *74*, 1007–1013.

CT900240S